ACS Chemical Neuroscience

Research Article

pubs.acs.org/chemneuro

Conformational Gating Dynamics in the GluCl Anion-Selective Chloride Channel

Özge Yoluk,[†,‡] Erik Lindahl,[†,‡,§] and Magnus Andersson*[,†,‡]

[†]Science for Life Laboratory, Stockholm and Uppsala, 171 21 Stockholm, Sweden

[‡]Theoretical and Computational Biophysics, Department of Theoretical Physics, KTH Royal Institute of Technology, 106 91 Stockholm, Sweden

[§]Department of Biochemistry and Biophysics, Center for Biomembrane Research, Stockholm University, 114 18 Stockholm, Sweden

Supporting Information

ABSTRACT: Cys-loop receptors are central to propagation of signals in the nervous system. The gating of the membrane-spanning pore is triggered by structural rearrangements in the agonist-binding site, located some 50 Å away from the pore. A sequential conformational change, propagating from the ligand-binding site to the pore, has been proposed to govern gating in all Cys-loop receptors. Here, we identify structural and dynamic components of the conformational gating in the eukaryotic glutamate-gated chloride channel (GluCl) by means of molecular dynamics (MD) simulations with and without the L-glutamate agonist bound. A significant increase in pore opening and accompanying hydration is observed in the presence of glutamate. Potential of mean force calculations reveal that the barrier for ion passage drops from 15 kcal/mol to 5−10 kcal/mol with the agonist bound. This appears to be explained by agonist binding that leads to significant changes in the intersubunit hydrogen-bonding pattern, which induce a slight tilt of the extracellular domain relative to the transmembrane domain in the simulations. This rearrangement is subtle, but correspond to the direction of the quaternary twist observed as a key difference between open and closed X-ray structures. While the full reversible gating is still a much slower process, the observed structural dynamics sheds new light on the early stages of how the agonist influences the extracellular domain, how the extracellular domain interacts with the transmembrane domain, and how changes in the transmembrane domain alter the free energy of ion passage.

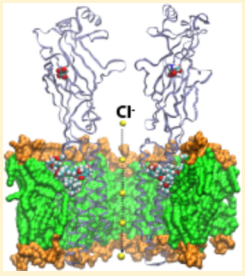

KEYWORDS: *Membrane protein, ligand-gated ion channel, cys-loop receptor, molecular dynamics simulations*

Cys-loop receptors are important components of the nervous system, and their malfunction is associated with various neurological disorders, such as depression, epilepsy, and startle disease.[1] These channels are also central in drug addiction research since compounds such as ethanol, barbiturates, nicotine, and cannabinoids bind in both the extracellular and transmembrane domains and affect the gating mechanism via allosteric modulation.[2,3] Therefore, the search for the fundamental principles that underlie gating of these channels has attracted major academic and pharmaceutical research efforts. The first high-resolution Cys-loop crystal structures were obtained for the bacterial homologues ELIC[4] and GLIC.[5−7] This provided an important structural framework by which to interpret experimental observations from the eukaryotic channels. In 2011, the crystal structures of GluClα (glutamate-gated chloride channel (GluCl)) presented the first high-resolution view of a eukaryotic Cys-loop receptor.[8] Recently, X-ray structures were presented of the homopentameric 5HT3-A[9] and the GABA$_A$-β3 receptor,[10] as well as a closed state of GluClα.[11] Because the two open state GluClα crystal structures represent different degrees of activation with minimal differences in the crystallization conditions, these structures are highly suitable systems in which to monitor gating using molecular dynamics (MD) simulations. In addition, the GABA$_A$-β3 structure likely represents a desensitized state[10] and simulating activation of the closed state GluClα[11] and the presumably nonconducting 5HT3-A[9] structures would require very long simulation time scales. The 34% sequence identity to GlyR suggests a shared global fold for GluClα, which corresponds to a pentameric structure where each subunit consists of a large, β-sheet-rich, extracellular domain (ECD) and a 4-helical transmembrane domain (TMD). The ECD contains the agonist-binding site, and the TMD consists of four TM helices (M1−M4), where the membrane-spanning ion pore is found. The ECD contains loop regions that induce connectivity both between the principal (+) and complementary (−) subunits as well as to the membrane region, where the latter ECD−TMD interface has been implicated as crucial to the gating mechanism.[12−14]

While the most common forms of the human anion-selective Cys-loop receptors GABA$_A$R and GlyR are heteropentamers, the invertebrate GluCl receptor exists in heteromeric as well as homopentameric assemblies. Because uncovering gating dynamics from a background of general protein structural dynamics is a daunting task, a target with five identical subunits is an ideal starting point to explore the mechanisms of the internal signaling pathway. However, even within GluCl

Received: April 8, 2015
Revised: May 19, 2015
Published: May 20, 2015

DOI: 10.1021/acschemneuro.5b00111
ACS Chem. Neurosci. 2015, 6, 1459−1467

homopentamers there are variations depending on whether the assembly consists of α- or β-subunits. GluClβ is directly gated by glutamate,[15] while GluClα requires the presence of ivermectin (IVM),[16] a broad-spectrum antiparasitic agent used to control parasitic nematodes in humans and animals.[17,18] Ivermectin is a partial allosteric agonist that activates GluClα by structural stabilization,[8,19] which paves way for further activation by glutamate.[16] In principle, the structural network responsible for mediating the signal between the agonist-binding site and the membrane pore could be identified by looking at differences between the crystal structures of IVM-activated GluClα channels in the presence and absence of glutamate.

In the search for the structural components involved in gating, two major features stand out when comparing the crystal structures representing conformations of the proton-gated GLIC channel trapped at different pH values,[7] which were the first structures captured in different states. The extracellular halves of TMD helix M2 showed significant inward tilting to seal the pore at high pH. The interfaces between subunits as well as the ECD−TMD interfaces, incorporating the M2-M3 and Cys loops, were also reshaped. There is plenty of evidence reporting similar structural features from a wide range of different experimental techniques, such as electron paramagnetic resonance (EPR) spectroscopy,[20] electrophysiology,[21] and rate-equilibrium free-energy relationship (REFER) analyses, where the latter have provided information on the direction and order of local structural features involved in the gating mechanism (reviewed in ref 12). MD simulation approaches have focused on adding high-resolution dynamic information to the framework provided by the experimental efforts. Structural rearrangements of TMD helix M2 have been observed to influence the ion pore in almost all simulations of full-length (including both the ECD and TMD) Cys-loop receptors, for example, for ELIC,[22] GLIC,[23] homology models of GlyR,[24] and the human nAChR[25,26] (although many of these likely reflect pore collapse, since M2 closure was observed even under conditions where the channel should conduct). In addition, attempts have been made to monitor nonequilibrium gating dynamics by introduction of a trigger intended to induce the gating mechanism. For instance, the pH-gated GLIC channel responded to a simulated pH-jump by closing tilts of M2 helices and subsequent ECD twist that were asymmetric in-between subunits.[27] Targeted MD was also used to close the agonist-binding site in the nAChR protein by forcing loop C inward, which partly opened the pore via the ECD β1-β2 loop.[28] A recent study of GluClα monitored dynamics after removal of bound IVM and observed agonist unbinding to close the ion pore via structural rearrangements at the β1-β2/M2-M3 interface.[29]

To avoid introducing bias from large perturbations, we attempt to study the conformational changes related to gating by comparing dynamics between intact crystal structures of IVM-activated GluClα channels in the presence and absence of glutamate. The overall conformations of the crystal structures are extremely similar (backbone rmsd = 0.24 Å) with only a few side chains showing significant reorientations; Arg56 in loop D and Tyr200 in loop C differ by 0.5 Å.[8] The inherent dynamical response might be subdued by the surrounding crystal lattice, in which case more pronounced effects on the protein dynamics might be exposed by allowing the crystal structures to equilibrate in a membrane environment. Therefore, in this work, we use 10 single-microsecond MD simulations of GluClα in dioleoylphosphocholine (DOPC) lipid bilayers in the presence and absence of bound glutamate (Figure 1) to contrast their behavior. Pore radius analyses showed a 1−3 Å increase in the minimum pore radius in the presence of glutamate. Estimated relative free energies by potential of mean force (PMF) calculations also appeared to be coupled to a free energy barrier that was reduced from 15 kcal/mol to 5−10 kcal/mol. The radius in the TMD ion pore was correlated with the quaternary twist of the ECD relative to the TMD upon agonist binding. This suggests that both the twist motion and the increase in pore radius could be the result of changes in hydrogen-bonding network originating from the agonist-binding site.

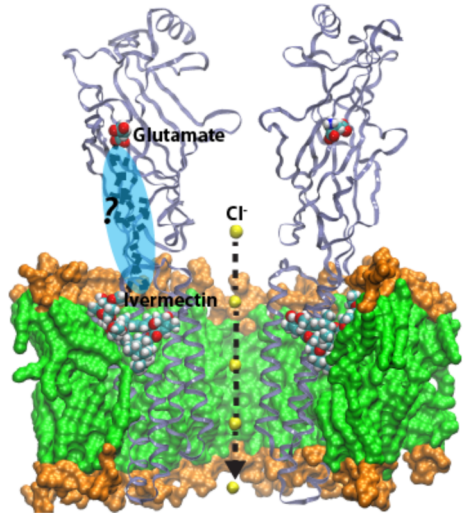

Figure 1. Cartoon visualizing two subunits of the GluCl pentamer. The polar lipid headgroups and apolar acyl chains of the DOPC lipid bilayer are represented as van der Waals surfaces. Glutamate and ivermectin molecules are represented in their crystallographic positions. Chloride ions delineate the membrane pore.

RESULTS

In the following sections, we compare the results from 10 single-microsecond MD simulations. Five of these were based on the unligated GluClα channel (−GLU, sim1−5), and the remaining five simulations described the ligated channel (+GLU, sim1−5). In addition, we performed a 600 ns control simulation where L-glutamate was removed from +GLU sim4, which showed the most prominent pore opening (rGLU). The ligand occupancy in the five +GLU simulations were 88% (sim 1), 81% (sim 2), 74% (sim 3), 85% (sim 4), and 67% (sim 5), respectively (Table S1, Supporting Information) with the glutamate ligand present in the ligand-binding site in at least three of the subunits and showing repeated unbinding/rebinding events in the remaining subunits (Figure S1).

Agonist Binding Increases Pore Radius and Facilitates Anion Passage. Starting from the −GLU and +GLU open crystal structures, all simulations displayed significant constriction at the hydrophobic 9′ girdle immediately after releasing the restraints. While the −GLU simulations maintained this constriction, three out of five +GLU simulations showed significant opening in the 9′ region and in one simulation (+GLU sim4) even reestablishing the open crystal structure dimensions. To identify structural effects of the presence of glutamate on the ion-conducting pore, we first

DOI: 10.1021/acschemneuro.5b00111
ACS Chem. Neurosci. 2015, 6, 1459−1467

calculated the minimum pore radius position (Figure 2A, B) and the pore radius at the 9′ position (between −2.5 and 2.5

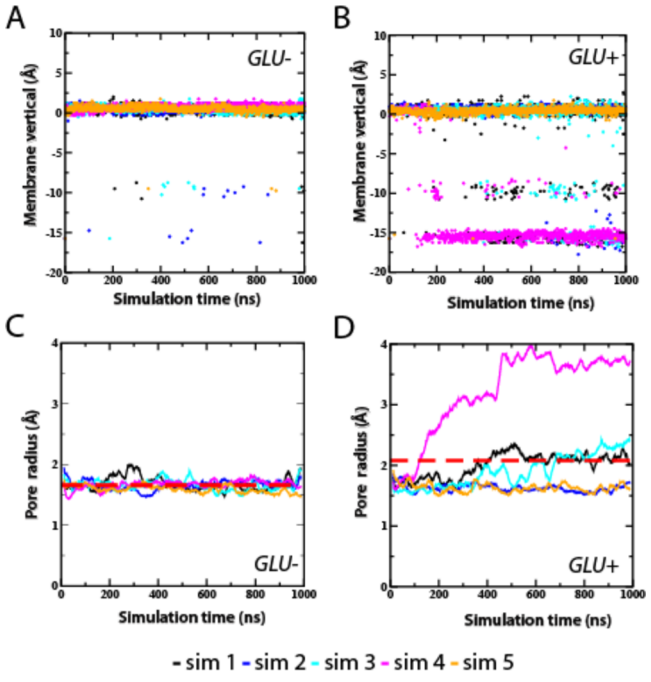

Figure 2. Structural dynamics in the membrane pore region is ligand dependent. The positions of the minimum pore radii with respect to the vertical of the membrane are displayed as a function of simulation time for five simulation systems in the absence (-GLU) (A) and presence (+GLU) (B) of L-glutamate ligands, respectively. The accompanying minimum pore radii are shown for the -GLU (C) and +GLU (D) simulations, respectively. The dashed lines correspond to an average of the five independent simulations for each condition with or without GLU.

Å), which corresponds to the constriction point in the closed state (PDB ID 4TNV)[11] (Figure 2C, D). Because the ECD is lacking constricted regions for the pore, we focused our analyses on the transmembrane region. Agonist binding to the orthosteric site appeared to shift the structural configuration of the transmembrane domain toward a more open state. The intracellular half of the GluCl pore contains the selectivity filter located at positions −1′ Ala and −2′ Pro. In +GLU simulations, the constriction point was located at the selectivity filter instead of 9′ (Figure 2B), which is reminiscent of open state GLIC structures.[5] In some simulations (+GLU sim1/3/4), the average pore radius at 9′ even exceeded the effective ion radius of Cl^- of 1.8 Å (Figure 2D).

The positions of the pore constriction points (Figure 2A-B), the pore radii at 9′ (Figure 2C−D), and the pore radius profiles (Figure 3A-B) revealed three distinct states of the transmembrane domain: "open" (+GLU sim4), "half-open" (+GLU sim1 and sim3), and "closed ligated/unligated" (-GLU sim1−5, +GLU sim2/5). To determine the energy barriers associated with passage of a Cl^- ion through the ion-conducting pore, we performed potential of mean force (PMF) calculations starting from average structures of three simulations, each representative of the open, half-open and closed states of the transmembrane domain, respectively. The starting position on the extracellular side was defined from the center-of-mass of the conserved residue Arg 211 in TM helix M1 from each subunit. The Cl^- ion was then pulled at a rate of 5 Å/ns through the

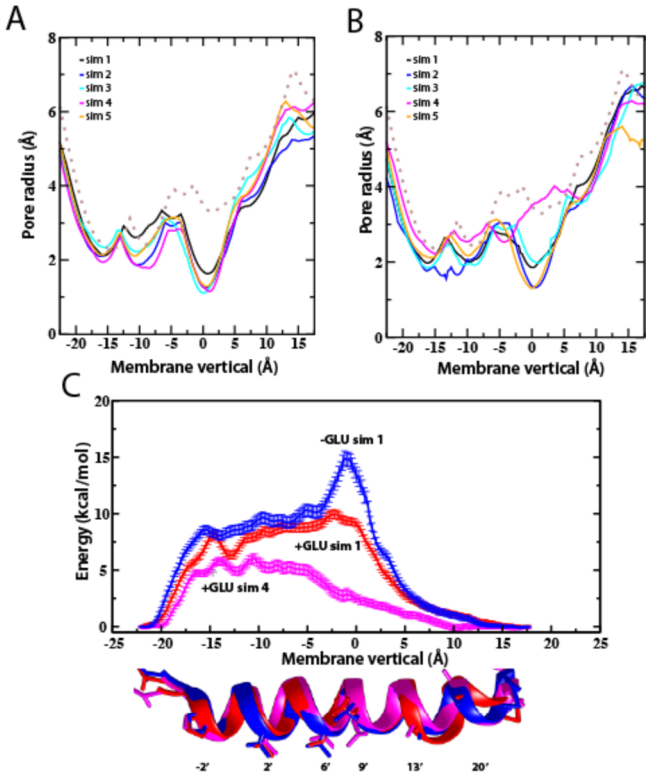

Figure 3. Ligand-dependent structural rearrangements in the pore affect the barrier for ion passage. The pore radii corresponding to representative averages in the final 500 ns of simulation are shown for the systems in the absence (A) and presence (B) of the glutamate ligand. The pore radius of the open state crystal structures is shown in dashed lines and is represented by the GLU-containing GluClα (PDB ID: 3RIF) due to the low backbone RMSD (0.24 Å) compared to the structure without GLU (PDB ID: 3RHW). The PMF profiles for Cl^- passage are shown in (C) for a system in the absence of GLU (−GLU sim 1, "closed unligated"), and two simulations in the presence of GLU (+GLU sim 1, "half-open"; +GLU sim 4, "open").

pore to the cytoplasmic side. The free energies reported from the open (+GLU sim4), half-open (+GLU sim1), and closed (−GLU sim1) states differed significantly at the 9′ constriction point (Figure 3C). In fact, a three times higher force constant was required to keep the ion from moving toward more favorable regions in the −GLU sim1 for PMF windows between 6′ and 9′ positions. The passage of Cl^- through the pore in the absence of glutamate was associated with an energetic penalty of more than 15 kcal/mol, but in the systems with glutamate bound this was reduced significantly to 5−10 kcal/mol, largely due to the increased radius in the most constricted part of the pore. While some caution is advised when drawing conclusions about the specific free energy values for the barriers, it is interesting that the simulations indicate clear effects from binding of glutamate in the orthosteric site on Cl^- ion passage in the pore some 50 Å away, in particular at the 9′ position.

Glutamate Binding Alters the Hydrogen Bond Network. Agonist binding appeared to facilitate the formation of intersubunit interactions within the orthosteric site. To determine the effect of agonist binding on specific interactions, we calculated the average hydrogen bond occupancy for both −GLU and +GLU systems using the H-bond plugin of VMD (Visual Molecular Dynamics).[30] In order to reduce the noise, we applied two filters: First, residue pairs with occupancies less

DOI: 10.1021/acschemneuro.5b00111
ACS Chem. Neurosci. 2015, 6, 1459−1467

than 10% were removed in all three systems, −GLU, +GLU, and rGLU. Second, we only focused on residue pairs where the difference between −GLU and +GLU systems exceeded 5%. The resulting occupancies from the −GLU, +GLU, and rGLU systems were then compared using one-way ANOVA statistical analyses in which simulation time (ns) was taken as N and the confidence interval was chosen as 0.05 (p-value). In this way, the presence of the glutamate ligand was observed to alter the probability of hydrogen-bond formation for 10 intersubunit and 53 intrasubunit residue pairs (Tables S2 and S3). Several of the hydrogen bond interactions that resulted in the most significant changes in-between simulations with and without glutamate were also confirmed to reverse when the glutamate was removed in the control rGLU simulation. While this observation strengthens the overall conclusions, it should not be overinterpreted given significantly less sampling in the control simulation.

Agonist Binding Rearranges Intersubunit Hydrogen Bonds at the Orthosteric Site. The changes in intersubunit hydrogen-bond interactions were located mainly in the vicinity of the orthosteric site. A full list of intersubunit interactions that resulted in significant change in-between −GLU and +GLU simulations is reported in Table S2. In the absence of the glutamate agonist, R37 of the principal subunit (loop G) was interacting with the backbone of residues P93 and E95 in loop A in the complementary subunit (Figure 4, −GLU). In the presence of the agonist, R37 became disconnected from loop A (Figure 4. +GLU). In addition, intersubunit interactions between Y151 (Loop B) of the principal subunit and T54 (loop D) and S121 (loop E) of the complementary subunit were induced in the presence of the ligand. The Y151 residue in loop B is highly conserved and in several LGICs the aromatic side chain has been proposed to be involved in cation−π interaction with the agonist.[31,32] Indeed, we observed the distance between the Y151 and Y200 aromatic rings and the amino group of the glutamate ligand to be within range for cation−π interactions (Figure S1). It is important to note however that such interactions are not explicitly described in classical force fields.

In contrast to residues R37, Y151, and S121, which were all directly interacting with the ligand, the interaction dynamics of residue N196 (loop C) was shifted toward Q169 (loop F) in the neighboring subunit without involving direct glutamate interactions. We have previously reported loop C to become disordered in the presence of ivermectin in the allosteric site.[19] We now note that agonist binding induce the opposite effect; an increased frequency of the intersubunit N196-Q160 interaction leads to the stabilization of loop C. Finally, we observed residues R17 ($\alpha1/\beta1$ loop) and G82 ($\beta3/\beta4$ loop) to interact more in the presence of the ligand. In summary, agonist binding promoted interactions between residue pairs R17-G82, Y151-T54, Y151-S121, and N196-Q169 while reducing interactions P93-R37 and E95-R37.

Changes in the Intrasubunit Interaction Patterns upon Agonist Binding. Similar to the interactions in-between subunits, the intrasubunit interactions that were most affected by the ligand were found mainly in proximity to the orthosteric site (Table S3). One of the major intrasubunit interactions induced by the presence of L-glutamate was between R56 (loop D) and Q169 (loop F) (Figure 5). The observed signal in-between simulations were highly significant and the control simulation resulted in full recovery of the conditions without L-glutamate. In addition, we

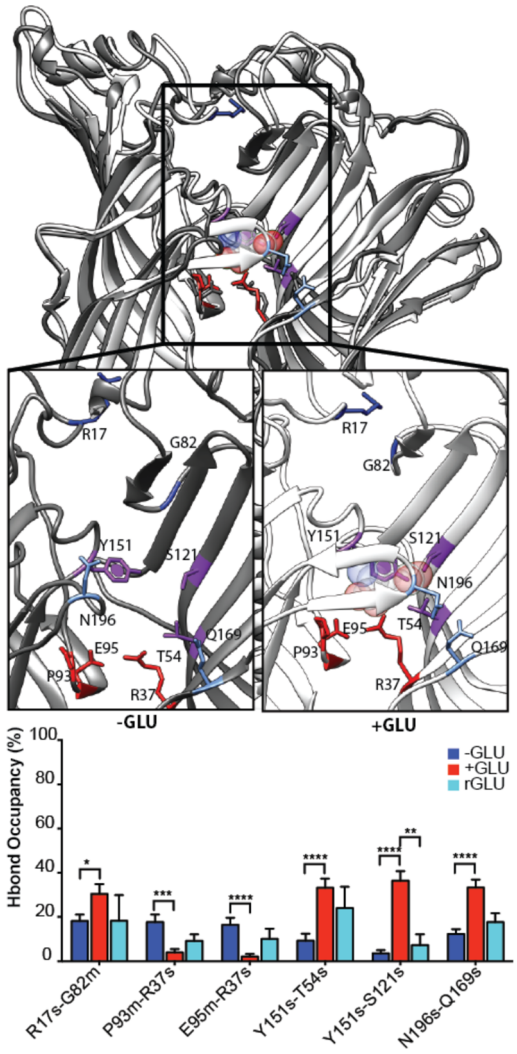

Figure 4. Agonist binding affects intersubunit interactions. Representative states from "closed" (−GLU sim4) and "open" (+GLU sim4) simulations are shown superimposed in gray and white, respectively. The orthosteric ligand-binding site is highlighted for both states showing intersubunit residues that displayed significant differences in their interaction patterns related to the presence or absence of the glutamate ligand. The average H-bond occupancies for all simulations in the absence (−GLU) and presence (+GLU) of glutamate and the control simulation (rGLU) are shown in the histogram. Notations *, **, ***, and **** represent p-values of 0.05, 0.01, 0.001, and 0.0001, respectively; s = side chain, and m = main chain.

observed a structural transition in Loop F localized further toward the transmembrane domain. While this loop had at least some helical content in the absence of L-glutamate, it became significantly unstructured upon ligand binding (Table S3, Figure S2). An additional change in the intrasubunit connections was found between Y151 (loop B) and D89 (loop A) (Figure 5). Upon L-glutamate binding there was a significant drop in the D89-Y151 hydrogen bond frequency, which reflects our observed increase in L-glutamate and intersubunit interactions of the Y151 residue. Not all interactions were reversed in the control simulation, but given the relatively slow gating process we do not expect microsecond-scale simulations to reproduce the complete process, in particular not reversibly. In summary, agonist binding decreased hydrogen bond interactions for residue pairs

DOI: 10.1021/acschemneuro.5b00111
ACS Chem. Neurosci. 2015, 6, 1459−1467

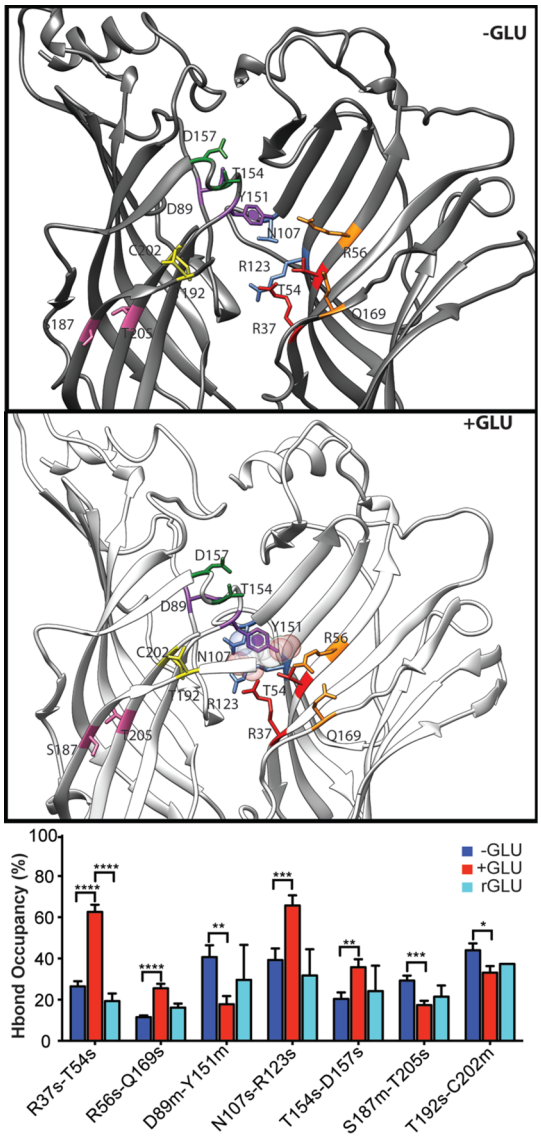

Figure 5. Agonist binding influence on intrasubunit interactions. Representative states from "closed" (−GLU sim4) and "open" (+GLU sim4) simulations are shown in gray and white, respectively, focusing on the orthosteric ligand-binding site. Residues showing high degrees of variability depending upon the presence or absence of L-glutamate are highlighted. The average H-bond occupancies for all simulations in the absence (−GLU) and presence (+GLU) of glutamate and the control simulation (rGLU) are shown in the histogram. Notations *, **, ***, and **** represent *p*-values of 0.05, 0.01, 0.001, and 0.0001, respectively; s = side chain, and m = main chain.

simulations with and without L-glutamate; both simulations showed a 13° ± 0.4 twist angle of the ECD relative to the TM domain. This is close to the value of the GluCl open state crystal structure, while the closed state crystal structure has a 22° twist angle (Table S4).

Because our hydrogen bond analyses indicated significant dynamics peripheral to the core domain, we included β3-5, β8-9, and TM loops into the twist angle analyses. In addition, the change in the twist angle was monitored in the simulation that resulted in the largest dilation of the pore region (+GLU sim4). Here, a decrease in the twist angle (Figure 6A) was observed

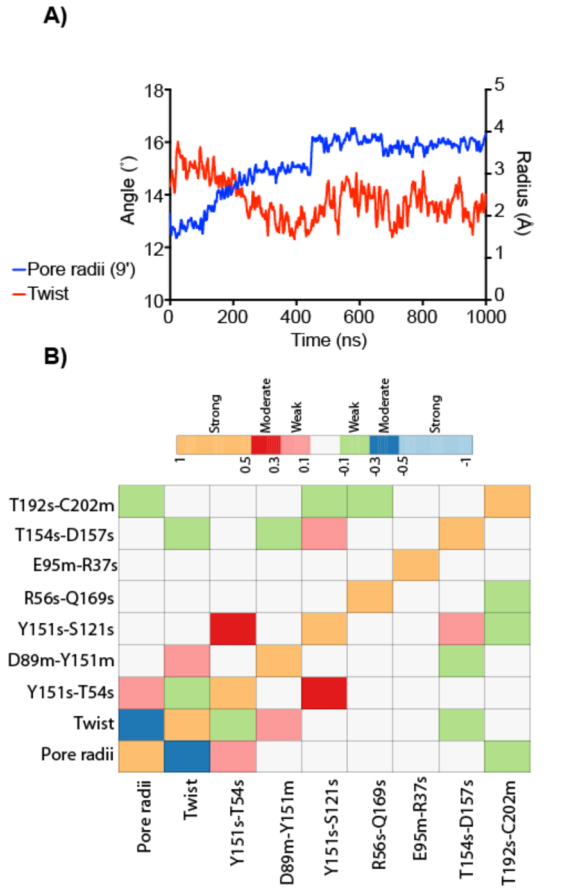

Figure 6. Altered subunit interactions lead to quaternary twist. (A) The 9′ pore radius and ECD-TM twist angle are shown as a function of simulation time. (B) Pearson correlation analysis showing correlations between hydrogen bond interactions, twist angle, and pore radii. For the hydrogen bonds, s indicates interactions with the side chain, and m the main chain.

on the principal subunits D89-Y151, S187-T205, and T192-C202, while increasing interactions between residue pairs on the complementary subunits R37-T54, R56-Q169, N107-R123, and T154-D157.

Agonist Binding Induces a Quaternary Domain Twist. Comparison of the GLIC open/closed state crystal structures revealed a change in quaternary twist of the ECD with respect to the TM segment,[7,33] which was also observed in-between the open/closed state crystal structures of GluCl.[11] A conserved core consisting of five β-strands in the ECD and the four TM α-helices was defined to allow comparison of structural dynamics in-between LGIC proteins.[29] Given this definition, we did not observe significant differences between our

that was moderately correlated with pore opening (Figure 6). While the experimental difference is clearly larger, the direction of the twist was correct. Therefore, the hydrogen bond dynamics in the ECD loop regions observed in the simulations might be responsible for inducing the domain rearrangement that ultimately opens the channel.

Pore Opening and ECD-TM Twist Shows Significant Correlation to Y151-T54 Interactions. It is inherently difficult to pinpoint specific gating dynamics especially since some structural rearrangements will be strictly involved in ligand binding, but not gating. To identify structural dynamics putatively involved in gating, we relied on statistical analyses. First, the average hydrogen bond occupancies between the

DOI: 10.1021/acschemneuro.5b00111
ACS Chem. Neurosci. 2015, 6, 1459−1467

−GLU, +GLU, and control rGLU simulations were compared using one-way ANOVA analyses with a confidence interval p-value of 0.05%. While these interaction pairs were all influenced by ligand binding to at least some degree, the question remained as to whether they were also involved in the gating process. We then selected residue pairs that showed a maximum difference in the total number of hydrogen bonds per residue pair in-between "open/half-open" simulations (+GLU sim1/3/4) and "closed" simulations (+GLU sim2/5) in a second round of one-way ANOVA analyses (underlined red in Tables S2 and S3). Due to extensive autocorrelation times in the MD trajectories (~200 ns), this ANOVA analysis merely functioned as a selection process to avoid the problem size exploding and we therefore refrain from claims about statistical significance. The identified interactions were then subjected to correlation analyses with respect to pore radius and twist angle within +GLU sim4 "open" state as it displayed the largest pore opening. This means that although there could be residue pairs left unidentified in the ANOVA selection process, the subsequent correlation analyses for the included pairs will be correct.

The following residue pairs showed were selected for further correlation analysis in the "open" (+GLU sim4) simulation: E95-R37, Y151-T54, Y151-S121, R56-Q169, D89-Y151, T154-D157, and C202-T192 (Figure S3, Table S5). Residue pairs E95-R37, Y151-S121, and R56-Q169 showed no correlation with pore opening or twist motion; for these, the glutamate-induced change in hydrogen-bond interactions might only be related to ligand binding. Of all interactions, correlation analysis indicated residue pairs Y151-T54, D89-Y151, T154-D157, and C202-T192 as putative gating contributors as they were correlated either with increase in pore radii or decrease in twist angle (Figure 6B). The interaction Y151-T54 was the only pair found to be correlated with the changes both in pore radius and twist angle (Figure 6B).

DISCUSSION

Complex salt-bridge/hydrogen-bond networks stabilize conformational states of membrane proteins. A structural perturbation, such as a deprotonation event or the binding of a ligand, can induce structural rearrangements in these hydrogen-bond networks that results in transition between conformational states.[34] However, determining such subtle rearrangements is challenging and requires a suitable methodology and model system. Because atomistic MD simulations can monitor both global and local structural dynamics of proteins inserted into a lipid environment, such methods are particularly attractive for characterizing structural transitions in membrane proteins. In this work, we contrast structural dynamics of GluClα in a set of microsecond simulations either with or without L-glutamate in an attempt to uncover structural rearrangements relevant for ligand binding and gating. By combining extensive sampling (10×1 μs), free energy calculations, and statistical analyses, we were able to identify a set of amino acid interactions that were correlated to ligand binding, gating or both.

Structural Rearrangements in the Membrane Pore. The GluClα crystal structures with or without glutamate differ only by subtle structural rearrangements.[8] The crystallization conditions might bias a certain conformation and hence prevent the full response of agonist binding. In addition to relieving strain in crystal structures, simulations can probe the conformational changes that would occur as a consequence of ligand binding that lead to actual gating. While we observed little variation in the pore region in our simulations without L-glutamate, the pore radius in 3 out of 5 simulations showed a significant increase with the ligand bound. Extensive sampling (at least 100−300 ns) was required for these conformational changes to occur.

The major pore dilation was located in the central 9′ region. The pore center (9′) hosts the hydrophobic girdle, which has been attributed a function as the gate controlling ion conduction across the pore.[35−37] In our simulations, the increased pore radius was mainly an effect of side-chain motions of the 9′ Leu residues after 100−300 ns simulation time with L-glutamate bound. A free energy barrier in the order of 15 kcal/mol was calculated for Cl^- transfer in the absence of glutamate at 9′, which was reduced to 5−10 kcal/mol with the agonist present. When using elastic network models to specifically create models with fully open pore states, even lower free energies have been observed.[38,39] Although our system does not yet represent a fully conducting channel, it appears that the simulations were able to capture the first stages of the process where extracellular agonist binding influences the transmembrane pore, without making any assumptions or steering the channel toward a more open state.

Agonist Binding Leads to Conformational Changes. The major secondary structural changes induced by agonist binding were located on loops C and F. Upon agonist binding, loop C became ordered (Figures 4 and 5) and loop F transitioned from helix to turn (Figure S2). Loop F has been observed to be involved in agonist binding[38,40] and was proposed to have a direct role in gating.[41,42] To our knowledge, structural dynamics identifying coupling between loop F conformational changes and structural effects in the transmembrane pore (Figure 6) have not yet been observed by means of simulation methods.

The binding pose of L-glutamate described by the crystal structure was well maintained in our simulations. Aromatic side chains in loops B (Y151) and C (Y200) were found to stabilize the ligand in its binding pocket with Y200 contributing slightly more than Y151 (Figure S1), which is in agreement with experimental data showing significantly reduced conductance in GluCl Y200 mutants probing the cation-π interaction.[43] Other channels (nAChR,[32] $GABA_A$-rho[31]) are sensitive to Y151 mutations, which indicates that both residues can be important, with some variations between channel types. In addition, the site corresponding to Y151 has also been found to be important in GluClβ, where mutation of this residue or its interaction partner in the neighboring subunit resulted in 800-fold and 590-fold reductions of channel activity, respectively.[43]

We observed the strongest differences for the Y151-T54 interaction. The residue Y151 is located in a highly flexible region, and there are a number of neighbor interactions that appear to help stabilize Y151 in this location, in particular Y151-S121, D89-Y151, and T154-D157. The interactions of D89 with this loop have been investigated in nAChR.[44,45] Cashin et al.[45] concluded that no single D89 interaction was essential for activity, but that the D89-loop B interactions help preorganize the agonist binding site.[45] While the main chain interactions of D89 changed during the twist motion in the simulations, we did not observe any significant correlation between D89 side chain interactions and the conformational change, which is in agreement with the experimental findings. The T154-D157 interaction was also well correlated with the interactions of Y151. A recent study in GlyR shows that

DOI: 10.1021/acschemneuro.5b00111
ACS Chem. Neurosci. 2015, 6, 1459−1467

replacing this Thr with a Met is associated with hyperplexia and decreased glycine affinity.[46]

Using statistical correlation analyses, we identified the Y151-T54 interaction as the most likely contributor to gating, and the only residue pair correlated with the ECD-TM twist motion (Figure 6B). Hence, the Y151-T54 interaction appears to act like a communication relay between subunits. Interestingly, while T54 is conserved in both *Caenorhabditis elegans* and *Drosophilia melanogaster* glutamate-gated ion channels,[47] the corresponding position in LGICs gated by GABA, glycine, or nicotine contains either a Tyr or a Phe residue (Figure S4). Mutations of Tyr or Phe to nonaromatic residues (Ala, Val, Cys, or Leu) were shown to decrease the EC_{50} in nAChR $\alpha7$[48] and $GABA_AR$[49] channels, suggesting a requirement for an aromatic residue at this position. This implies that the gating dynamics involves interactions between loop B and loop D with variations depending upon the specific channel. While GluCl channels convey this loop interaction using hydrogen-bond interactions, nAChR$\alpha7$ and $GABA_AR$ might rely on aromatic side chain interactions.

Earlier simulation studies of GluClα have monitored the structural rearrangements of channel deactivation following removal of the cocrystallized partial agonist ivermectin (IVM).[19,29] In contrast, our present study tracks the structural response to the presence of the ligand, that is, channel activation. Because IVM and glutamate both activates GluClα, a comparison between these studies can possibly hint to differences in the activation mechanism in-between the two ligands. IVM binds in an intersubunit pocket close to the ECD−TMD interface. Indeed, removing the IVM molecule resulted in quite dramatic structural rearrangements in the ECD-TMD interface: a change in ECD−TMD twist angle of ∼6°,[29] repositioning of P268 (i.e., the M2-M3 loop) with respect to V47 on the $\beta2$-$\beta3$ loop,[29] a decrease in intersubunit distances measured between Cα's of G281 (principal helix M3) and L218 (complementary helix M1).[19] Because these rearrangements were very subtle in our study of the glutamate activation (Figures 6A and S5), such structural responses might be specific to IVM. This may not be surprising given the location of the IVM binding site at the ECD−TMD interface. However, one IVM effect peripheral to the ECD−TMD interface has been observed; loop C in the vicinity of the ligand-binding site was significantly more disordered in the presence of IVM.[19] In contrast, loop C was on average more ordered in our ligated simulations compared to the unligated simulations (Figure S5). Therefore, while the ECD−TMD effects seem to be triggered by IVM, both IVM and GLU might induce structural changes in the vicinity of the ECD ligand-binding site.

In conclusion, the presented simulations support a multistage gating model composed of (i) agonist binding, (ii) an altered hydrogen bond network that causes a tilt/twist in the ECD, and finally (iii) motions transmitted to the TMD that were supported by experimental evidence from various LGIC proteins. While the present simulations are not yet capable of sampling the full gating process, they provide some of the first clear correlations between agonist binding, domain motion, and the barrier to ion passage.

METHODS

The crystal structures of GluClα cocrystallized with ivermectin (IVM) (PDB ID 3RHW) and glutamate (GLU) (PDB ID 3RIF) were used to construct systems with and without glutamate, respectively.[8] The system without glutamate was recently used as part of a study that focused on the effects of IVM stabilization.[19] We inserted the two crystal structures into previously relaxed DOPC lipid bilayer systems modeled with the Berger force field parameters.[50] After removal of overlapping lipids each system contained 304 DOPC lipids. The system without glutamate contained ∼32,500 waters in a hexagonal box with a 112 Å side and a 152 Å height. To achieve a salt concentration in the physiological range of 100 mM, 59 Na^+ and 69 Cl^- ions were added. The system with GLU contained ∼29 700 waters in a hexagonal box with a 112 Å side and 151 Å height. In this system, 54 Na^+ and 59 Cl^- ions were added to neutralize the system at a total concentration of 100 mM.

The AMBER99SB-ILDN[51] and Berger[50] force fields were used for the protein and lipids, respectively. Parameters for IVM were generated according to the procedure described by Yoluk et al.[19] Glutamate ligand parameters were obtained through modifications of Amber99SB-ILDN N-terminal glutamate parameters; carboxyl end partial charges were obtained from C-terminal glutamate and Cα and Hα partial charges were adjusted to achieve a total −1 charge of the molecule. Bonds, angles, and dihedrals were generated with the pdb2gmx tool in gromacs using AMBER99SB-ILDN force field parameters (Table S6).

The system without glutamate was minimized for 5000 steps excluding protein−protein nonbonded interactions, and another 10,000 steps including all interactions, followed by a three-step successive relaxation protocol; 1000 kJ/mol/nm^2 position restraints were applied first to all heavy atoms for 50 ns, then protein backbone for 10 ns, and finally Cα atoms for 10 ns. IVM was restrained during the first two equilibration steps. The system with glutamate was minimized for 10 000 steps including all interactions, and then relaxed in a series of three consecutive 10 ns simulations with position restraints (1000 kJ/mol/nm^2) applied to heavy atoms, protein backbone and Cα atoms, respectively. IVM was restrained during the first two equilibration steps and glutamate was restrained in all three steps. Using the equilibrated structures, five production runs were generated for both systems (−GLU, +GLU) with velocities generated by a random seed in Gromacs with the temperature set to 310 K. All simulations were run with Gromacs 4.5 and a 2 fs time step, using the LINCS algorithm to constrain all bond lengths.[52] Particle mesh Ewald (PME) electrostatics was used with a 10 Å cutoff.[53] For both systems protein and ligands, water and ions and lipids were coupled separately to temperature baths of 310 K using the Bussi velocity-rescaling thermostat.[54] Pressure was adjusted with a semi-isotropic Berendsen weak barostat[55] to a pressure of 1 bar with τ_P = 5 ps and compressibility 4.5 × 10^{-5} bar^{-1}. No position restraints were applied to either the protein or ligands in the production runs.

For the PMF calculations, the largest cluster centers identified by the single linkage clustering method implemented in the Gromacs package[52] (with a 0.16 nm cutoff, based on the RMSD distribution) from the second half of the production runs were chosen as starting points. A Cl^- ion was positioned at the ECD/TMD interface guided by the center-of-mass of the conserved residue Arg 211 for each subunit. Deletion of overlapping water molecules within 3 Å of the Cl^- ion was followed by a 10 ps nonrestrained simulation step to allow equilibration of the ion hydration shell. Equilibrated structures were then used for steered MD simulation where a pull rate of 5 Å/ns was applied to the Cl^- ion for 10 ns using the Gromacs pull code[52] with a direction along the normal to the lipid bilayer. A force constant of 1000 kJ/mol/nm^2 was applied to a reference group consisting of Arg 211 from the five subunits. The pull simulation resulted in start and end positions with respect to the Arg 211 reference point of 0.5 and 45 Å, respectively. In the umbrella sampling procedure, each 0.5 Å window was equilibrated for 100 ps with 1000 kJ/mol/nm^2 position restraints on the Cl^- ions followed by a 2 ns production run. For the system without GLU, additional sampling windows and a 3000 kJ/mol/nm^2 force constant were required for the 9′ region (−2.5 Å to 2.5 Å in Figure 3C) due to side-chain crowding. The PMF profiles were generated using the Weighted Histogram Analysis Method (WHAM)[56] implemented in the g_wham Gromacs tool. The extracellular domain was not included in the PMF calculations, and

DOI: 10.1021/acschemneuro.5b00111
ACS Chem. Neurosci. 2015, 6, 1459−1467

the g_wham analysis was performed using periodic option (cycl). Errors were estimated using bootstrap analysis. Histograms were generated with the autocorrelation (-ac) option to perform the bootstrap (-traj option).

All analyses were performed using Gromacs[52] or VMD.[30] The pore radius was computed using the HOLE software.[57] Secondary structure calculations were performed with STRIDE in VMD.[58] Secondary structure probability plots were generated in WebLogo[59,60] with weight set to 7, the number of possible secondary structures defined in STRIDE. Statistical tests (one-way ANOVA with post tests (Dunnet and Tukey) and the Pearson correlation analysis) were performed using GraphPad Prism version 6.0f for Mac (GraphPad Software, La Jolla CA). Molecular graphics were generated with VMD,[30] the UCSF Chimera package,[61] and POV-Ray.[62]

■ ASSOCIATED CONTENT

Supporting Information

Additional figures and tables showing cation−π interactions of L-glutamate with loop B and loop C, helicity of loop F upon agonist binding, hydrogen bond interactions in open/half-open ligated and closed ligated simulations, sequence alignment of loops D, A, and B, ivermectin response, fraction of time spent bound/unbound per L-glutamate, intersubunit interactions altered by L-glutamate binding, intrasubunit interactions altered by L-glutamate binding, twist angles of pGLICs, interactions that discriminate between closed ligated and open/half-open ligated simulations, and L-glutamate parameters. The Supporting Information is available free of charge on the ACS Publications website at DOI: 10.1021/acschemneuro.5b00111.

■ AUTHOR INFORMATION

Corresponding Author

*E-mail: magnus.andersson@scilifelab.se. Phone: +46 769 469872.

Author Contributions

The manuscript was written by contributions of all authors. All authors have given approval to the final version of the manuscript.

Funding

This work was funded by grants from Marie Curie Career Integration Grant (FP7-MC-CIG-618558), Magnus Bergvalls Stiftelse (2014-00170), and Åke Wibergs Stiftelse (M14-0245) to M.A., and the Swedish e-Science Research Center (SeRC), and the Swedish Research Council (2013-5901) to E.L.

Notes

The authors declare no competing financial interest.

■ ACKNOWLEDGMENTS

Computational resources were provided by the Swedish National Infrastructure for Computing (2014/11-33).

■ REFERENCES

(1) Sine, S. M., and Engel, A. G. (2006) Recent advances in Cys-loop receptor structure and function. *Nature 440*, 448−455.

(2) Howard, R. J., Trudell, J. R., and Harris, R. A. (2014) Seeking structural specificity: direct modulation of pentameric ligand-gated ion channels by alcohols and general anesthetics. *Pharmacol. Rev. 66*, 396−412.

(3) Olsen, R. W., Li, G. D., Wallner, M., Trudell, J. R., Bertaccini, E. J., Lindahl, E., Miller, K. W., Alkana, R. L., and Davies, D. L. (2014) Structural models of ligand-gated ion channels: Sites of action for anesthetics and ethanol. *Alcohol.: Clin. Exp. Res. 38*, 595−603.

(4) Hilf, R. J., and Dutzler, R. (2008) X-ray structure of a prokaryotic pentameric ligand-gated ion channel. *Nature 452*, 375−379.

(5) Bocquet, N., Nury, H., Baaden, M., Le Poupon, C., Changeux, J. P., Delarue, M., and Corringer, P. J. (2009) X-ray structure of a pentameric ligand-gated ion channel in an apparently open conformation. *Nature 457*, 111−114.

(6) Hilf, R. J., and Dutzler, R. (2009) Structure of a potentially open state of a proton-activated pentameric ligand-gated ion channel. *Nature 457*, 115−118.

(7) Sauguet, L., Shahsavar, A., Poitevin, F., Huon, C., Menny, A., Nemecz, A., Haouz, A., Changeux, J. P., Corringer, P. J., and Delarue, M. (2014) Crystal structures of a pentameric ligand-gated ion channel provide a mechanism for activation. *Proc. Natl. Acad. Sci. U. S. A. 111*, 966−971.

(8) Hibbs, R. E., and Gouaux, E. (2011) Principles of activation and permeation in an anion-selective Cys-loop receptor. *Nature 474*, 54−60.

(9) Hassaine, G., Deluz, C., Grasso, L., Wyss, R., Tol, M. B., Hovius, R., Graff, A., Stahlberg, H., Tomizaki, T., Desmyter, A., Moreau, C., Li, X. D., Poitevin, F., Vogel, H., and Nury, H. (2014) X-ray structure of the mouse serotonin 5-HT3 receptor. *Nature 512*, 276−281.

(10) Miller, P. S., and Aricescu, A. R. (2014) Crystal structure of a human GABAA receptor. *Nature 512*, 270−275.

(11) Althoff, T., Hibbs, R. E., Banerjee, S., and Gouaux, E. (2014) X-ray structures of GluCl in apo states reveal a gating mechanism of Cys-loop receptors. *Nature 512*, 333−337.

(12) Miller, P. S., and Smart, T. G. (2010) Binding, activation and modulation of Cys-loop receptors. *Trends Pharmacol. Sci. 31*, 161−174.

(13) Dacosta, C. J., and Baenziger, J. E. (2013) Gating of pentameric ligand-gated ion channels: structural insights and ambiguities. *Structure 21*, 1271−1283.

(14) Kash, T. L., Jenkins, A., Kelley, J. C., Trudell, J. R., and Harrison, N. L. (2003) Coupling of agonist binding to channel gating in the GABA(A) receptor. *Nature 421*, 272−275.

(15) Cully, D. F., Vassilatis, D. K., Liu, K. K., Paress, P. S., Van der Ploeg, L. H., Schaeffer, J. M., and Arena, J. P. (1994) Cloning of an avermectin-sensitive glutamate-gated chloride channel from Caenorhabditis elegans. *Nature 371*, 707−711.

(16) Etter, A., Cully, D. F., Schaeffer, J. M., Liu, K. K., and Arena, J. P. (1996) An amino acid substitution in the pore region of a glutamate-gated chloride channel enables the coupling of ligand binding to channel gating. *J. Biol. Chem. 271*, 16035−16039.

(17) Aziz, M. A., Diallo, S., Diop, I. M., Lariviere, M., and Porta, M. (1982) Efficacy and tolerance of ivermectin in human onchocerciasis. *Lancet 2*, 171−173.

(18) Campbell, W. C., Fisher, M. H., Stapley, E. O., Albers-Schonberg, G., and Jacob, T. A. (1983) Ivermectin: a potent new antiparasitic agent. *Science 221*, 823−828.

(19) Yoluk, O., Bromstrup, T., Bertaccini, E. J., Trudell, J. R., and Lindahl, E. (2013) Stabilization of the GluCl ligand-gated ion channel in the presence and absence of ivermectin. *Biophys. J. 105*, 640−647.

(20) Velisetty, P., Chalamalasetti, S. V., and Chakrapani, S. (2012) Conformational transitions underlying pore opening and desensitization in membrane-embedded Gloeobacter violaceus ligand-gated ion channel (GLIC). *J. Biol. Chem. 287*, 36864−36872.

(21) Parikh, R. B., Bali, M., and Akabas, M. H. (2011) Structure of the M2 transmembrane segment of GLIC, a prokaryotic Cys loop receptor homologue from Gloeobacter violaceus, probed by substituted cysteine accessibility. *J. Biol. Chem. 286*, 14098−14109.

(22) Cheng, X., Ivanov, I., Wang, H., Sine, S. M., and McCammon, J. A. (2009) Molecular-dynamics simulations of ELIC-a prokaryotic homologue of the nicotinic acetylcholine receptor. *Biophys. J. 96*, 4502−4513.

(23) Mowrey, D., Cheng, M. H., Liu, L. T., Willenbring, D., Lu, X., Wymore, T., Xu, Y., and Tang, P. (2013) Asymmetric ligand binding facilitates conformational transitions in pentameric ligand-gated ion channels. *J. Am. Chem. Soc. 135*, 2172−2180.

(24) Murail, S., Wallner, B., Trudell, J. R., Bertaccini, E., and Lindahl, E. (2011) Microsecond simulations indicate that ethanol binds between subunits and could stabilize an open-state model of a glycine receptor. *Biophys. J. 100*, 1642−1650.

DOI: 10.1021/acschemneuro.5b00111
ACS Chem. Neurosci. 2015, 6, 1459−1467

(25) Cheng, X., Ivanov, I., Wang, H., Sine, S. M., and McCammon, J. A. (2007) Nanosecond-timescale conformational dynamics of the human alpha7 nicotinic acetylcholine receptor. *Biophys. J. 93*, 2622−2634.
(26) Haddadian, E. J., Cheng, M. H., Coalson, R. D., Xu, Y., and Tang, P. (2008) In silico models for the human alpha4beta2 nicotinic acetylcholine receptor. *J. Phys. Chem. B 112*, 13981−13990.
(27) Nury, H., Poitevin, F., Van Renterghem, C., Changeux, J. P., Corringer, P. J., Delarue, M., and Baaden, M. (2010) One-microsecond molecular dynamics simulation of channel gating in a nicotinic receptor homologue. *Proc. Natl. Acad. Sci. U. S. A. 107*, 6275−6280.
(28) Cheng, X., Wang, H., Grant, B., Sine, S. M., and McCammon, J. A. (2006) Targeted molecular dynamics study of C-loop closure and channel gating in nicotinic receptors. *PLoS Comput. Biol. 2*, e134.
(29) Calimet, N., Simoes, M., Changeux, J. P., Karplus, M., Taly, A., and Cecchini, M. (2013) A gating mechanism of pentameric ligand-gated ion channels. *Proc. Natl. Acad. Sci. U. S. A. 110*, E3987−3996.
(30) Humphrey, W., Dalke, A., and Schulten, K. (1996) VMD: visual molecular dynamics. *J. Mol. Graphics 14* (33−38), 27−38.
(31) Lummis, S. C., D, L. B., Harrison, N. J., Lester, H. A., and Dougherty, D. A. (2005) A cation-pi binding interaction with a tyrosine in the binding site of the GABAC receptor. *Chem. Biol. 12*, 993−997.
(32) Xiu, X., Puskar, N. L., Shanata, J. A., Lester, H. A., and Dougherty, D. A. (2009) Nicotine binding to brain receptors requires a strong cation-pi interaction. *Nature 458*, 534−537.
(33) Taly, A., Delarue, M., Grutter, T., Nilges, M., Le Novere, N., Corringer, P. J., and Changeux, J. P. (2005) Normal mode analysis suggests a quaternary twist model for the nicotinic receptor gating mechanism. *Biophys. J. 88*, 3954−3965.
(34) Andersson, M., Bondar, A. N., Freites, J. A., Tobias, D. J., Kaback, H. R., and White, S. H. (2012) Proton-coupled dynamics in lactose permease. *Structure 20*, 1893−1904.
(35) Beckstein, O., and Sansom, M. S. (2006) A hydrophobic gate in an ion channel: the closed state of the nicotinic acetylcholine receptor. *Phys. Biol. 3*, 147−159.
(36) Ivanov, I., Cheng, X., Sine, S. M., and McCammon, J. A. (2007) Barriers to ion translocation in cationic and anionic receptors from the Cys-loop family. *J. Am. Chem. Soc. 129*, 8217−8224.
(37) Miyazawa, A., Fujiyoshi, Y., and Unwin, N. (2003) Structure and gating mechanism of the acetylcholine receptor pore. *Nature 423*, 949−955.
(38) Khatri, A., Sedelnikova, A., and Weiss, D. S. (2009) Structural Rearrangements in Loop F of the GABA Receptor Signal Ligand Binding, Not Channel Activation. *Biophys. J. 96*, 45−55.
(39) Cheng, M. H., and Coalson, R. D. (2012) Energetics and ion permeation characteristics in a glutamate-gated chloride (GluCl) receptor channel. *J. Phys. Chem. B 116*, 13637−13643.
(40) Pless, S. A., and Lynch, J. W. (2009) Ligand-specific conformational changes in the alpha1 glycine receptor ligand-binding domain. *J. Biol. Chem. 284*, 15847−15856.
(41) Newell, J. G., and Czajkowski, C. (2003) The GABA(A) receptor alpha(1) subunit Pro(174)-Asp(191) segment is involved in GABA binding and channel gating. *J. Biol. Chem. 278*, 13166−13172.
(42) Thompson, A. J., Padgett, C. L., and Lummis, S. C. R. (2006) Mutagenesis and molecular modeling reveal the importance of the 5-HT3 receptor F-loop. *J. Biol. Chem. 281*, 16576−16582.
(43) Daeffler, K. N., Lester, H. A., and Dougherty, D. A. (2014) Functional evaluation of key interactions evident in the structure of the eukaryotic Cys-loop receptor GluCl. *ACS Chem. Biol. 9*, 2283−2290.
(44) Lee, W. Y., and Sine, S. M. (2004) Invariant aspartic Acid in muscle nicotinic receptor contributes selectively to the kinetics of agonist binding. *J. Gen. Physiol. 124*, 555−567.
(45) Cashin, A. L., Torrice, M. M., McMenimen, K. A., Lester, H. A., and Dougherty, D. A. (2007) Chemical-scale studies on the role of a conserved aspartate in preorganizing the agonist binding site of the nicotinic acetylcholine receptor. *Biochemistry 46*, 630−639.
(46) Schaefer, N., Kluck, C. J., Price, K. L., Meiselbach, H., Vornberger, N., Schwarzinger, S., Hartmann, S., Langlhofer, G., Schulz, S., Schlegel, N., Brockmann, K., Lynch, B., Becker, C. M., Lummis, S. C., and Villmann, C. (2015) Disturbed neuronal ER-Golgi sorting of unassembled glycine receptors suggests altered subcellular processing is a cause of human hyperekplexia. *J. Neurosci. 35*, 422−437.
(47) Dent, J. A. (2006) Evidence for a diverse Cys-loop ligand-gated ion channel superfamily in early bilateria. *J. Mol. Evol. 62*, 523−535.
(48) Gay, E. A., Giniatullin, R., Skorinkin, A., and Yakel, J. L. (2008) Aromatic residues at position 55 of rat alpha7 nicotinic acetylcholine receptors are critical for maintaining rapid desensitization. *J. Physiol. 586*, 1105−1115.
(49) Sigel, E., Baur, R., Kellenberger, S., and Malherbe, P. (1992) Point mutations affecting antagonist affinity and agonist dependent gating of GABAA receptor channels. *EMBO J. 11*, 2017−2023.
(50) Berger, O., Edholm, O., and Jahnig, F. (1997) Molecular dynamics simulations of a fluid bilayer of dipalmitoylphosphatidylcholine at full hydration, constant pressure, and constant temperature. *Biophys. J. 72*, 2002−2013.
(51) Lindorff-Larsen, K., Piana, S., Palmo, K., Maragakis, P., Klepeis, J. L., Dror, R. O., and Shaw, D. E. (2010) Improved side-chain torsion potentials for the Amber ff99SB protein force field. *Proteins 78*, 1950−1958.
(52) Pronk, S., Pall, S., Schulz, R., Larsson, P., Bjelkmar, P., Apostolov, R., Shirts, M. R., Smith, J. C., Kasson, P. M., van der Spoel, D., Hess, B., and Lindahl, E. (2013) GROMACS 4.5: a high-throughput and highly parallel open source molecular simulation toolkit. *Bioinformatics 29*, 845−854.
(53) Essmann, U., Perera, L., Berkowitz, M., Darden, T., Lee, H., and Pedersen, L. (1995) A smooth particle mesh Ewald method. *J. Chem. Phys. 103*, 8577−8593.
(54) Bussi, G., Donadio, D., and Parrinello, M. (2007) Canonical sampling through velocity rescaling. *J. Chem. Phys. 126*, 014101.
(55) Berendsen, H. J. C., Postma, J. P. M., van Gunsteren, W. F., DiNola, A., and Haak, J. R. (1984) Molecular dynamics with coupling to an external bath. *J. Chem. Phys. 81*, 3684−3690.
(56) Kumar, S., Rosenberg, J., Bouzida, D., Swendsen, R., and Kollman, P. (1992) THE weighted histogram analysis method for free-energy calculations on biomolecules. I. The method. *J. Comput. Chem. 13*, 1011−1021.
(57) Smart, O. S., Neduvelil, J. G., Wang, X., Wallace, B. A., and Sansom, M. S. (1996) HOLE: A program for the analysis of the pore dimensions of ion channel structural models. *J. Mol. Graphics 14* (354−360), 376.
(58) Frishman, D., and Argos, P. (1995) Knowledge-based protein secondary structure assignment. *Proteins 23*, 566−579.
(59) Crooks, G. E., Hon, G., Chandonia, J. M., and Brenner, S. E. (2004) WebLogo: a sequence logo generator. *Genome Res. 14*, 1188−1190.
(60) Schneider, T. D., and Stephens, R. M. (1990) Sequence logos: a new way to display consensus sequences. *Nucleic Acids Res. 18*, 6097−6100.
(61) Pettersen, E. F., Goddard, T. D., Huang, C. C., Couch, G. S., Greenblatt, D. M., Meng, E. C., and Ferrin, T. E. (2004) UCSF Chimera—A visualization system for exploratory research and analysis. *J. Comput. Chem. 25*, 1605−1612.
(62) Persistence of Vision Pty. Ltd. (2004) *Persistence of Vision Raytracer*, Version 3.6, Persistence of Vision Pty. Ltd., Williamstown, Victoria, Australia.

DOI: 10.1021/acschemneuro.5b00111
ACS Chem. Neurosci. 2015, 6, 1459−1467